Supplementary Materials for

A Bioinspired Strategy for Directional Charge Propagation in Photoelectrochemical Devices Using Supramolecular Machinery

Tessel Bouwens,[a] T. M. A. Bakker, [a] J. Hasenack, M. Dieperink, [a] Simon Mathew [a] and Joost N. H. Reek* [a]

[a] Homogeneous, Supramolecular and Bio-Inspired Catalysis, van 't Hoff Institute for Molecular Sciences, University of Amsterdam, Science Park 904, 1098XH Amsterdam (The Netherlands).

Email: j.n.h.reek@uva.nl

Contents

1. Synthesis of compounds and Characterization

S1.1. General

Commercially reagents and solvents were obtained Sigma-Aldrich and Fluorochem and were used without purification. Conducting FTO glass was obtained from Solaronix (L × W × D 100 ×100 mm × 2.3 mm, surface resistivity 15 Ω cm^{-2}) All reactions were carried out under nitrogen in flame dried glassware. MeCN, DCM, and THF were dried by a solvent purification system. Thin layer chromatography was performed on Merck KGaA aluminum plates pre-coated TLC silica gel 60 F_{254} and analyzed with UV light (254 nm and 365 nm). Column chromatography was performed using silica gel (SiliCycle, SiliaFlash P60, 40–63 μm, 230–400 mesh). NMR analysis was performed on a Bruker AV300, AV400 and AV500 spectrometer and are reported in ppm using a solvent residual signal as internal standard (7.26 ppm for $CDCl_3$; 5.32 ppm for CD_2Cl_2 and 2.05 ppm for $(CD_3)_2CO$). Exact mass of the compounds was obtained on an AccuTOF GC v 4g, JMS-T100GCV Mass spectrometer (JEOL, Japan) equipped with an FD Emitter, Carbotec or Linden (Germany), FD 13 μm. Current rate 51.2 mA min^{-1} over 1.2 min machine using field desorption (FD) as ionization method. UV–Vis measurements were performed on a single beam Hewlett Packard 8453 spectrometer in a 10 mm path length quartz cuvette using MeCN as background. Electrochemistry experiments were performed on a PGSTAT302N potentiostat from Autolab with a glassy carbon working electrode (MetrOhm, diameter 3 mm), a leakless Ag/AgCl reference electrode (eDAQ, ET069) and a Pt wire counter electrode. The 0.5 mM analyte solution contained 100 mM $TBAPF_6$ as supporting electrolyte and was prepared in absence of air. To all samples ferrocene/ferrocenium (Fc/Fc^+) was added as an internal redox standard to determine the redox potentials versus NHE ($E_{1/2}$ Fc/Fc^+ = 630 mV in MeCN[1] and 700 mV in DCM[2])

S1.2. Synthesis

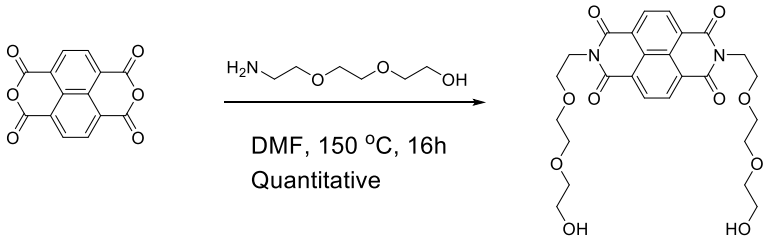

3-NDI-thread

3-NDI-thread: In a dried schlenk, 1,4,5,8-naphthalenetetracarboxylic dianhydride (1.02 g, 3.8 mmol, 1 eq.) and 2-(2-(2-aminoethoxy)ethoxy)ethoxy)ethan-1-ol (1.3 mL, 1.3 g, 8.8 mmol, 2.3 eq.) were dissolved in dry DMF (30 mL) This yellow solution was stirred for 16h at 150°C resulting in a black mixture. TLC (DCM:MeOH, 19:1 v/v) confirmed quantitative conversion to the final product. After cooling to room temperature, DMF was removed by rotary evaporation and the remaining brown solid was dissolved in $CHCl_3$ (150 mL). The organic layer was washed with water (3 × 150 mL) and subsequently dried ($MgSO_4$). Removal of the solvents afforded the product as a light brown crystalline solid (2.0 g, Quantitative yield). mp: 114.9°C; ^{1}H NMR (300 MHz, $CDCl_3$) δ 8.76 (s, 4H), 4.47 (t, *J* = 5.7 Hz, 4H), 3.87 (t, *J* = 5.7 Hz, 4H), 3.78 – 3.66 (m, 4H), 3.66 – 3.59 (m, 8H), 3.58 – 3.47 (m, 4H), 1.26 (s, 2H); ^{13}C NMR (75 MHz, $CDCl_3$) δ 163.11, 131.19, 126.91, 126.75, 77.36, 72.51, 70.57, 70.29, 68.04, 61.85, 39.78; FD–MS (MeCN) *m/z*: calculated for $C_{26}H_{30}N_2O_{10}$ [M^+]: 530.1900. Found 530.1905; FT–IR (neat): 3406, 2919, 2871, 1706, 1665, 1580, 1335, 1245, 1102, 1063, 768.

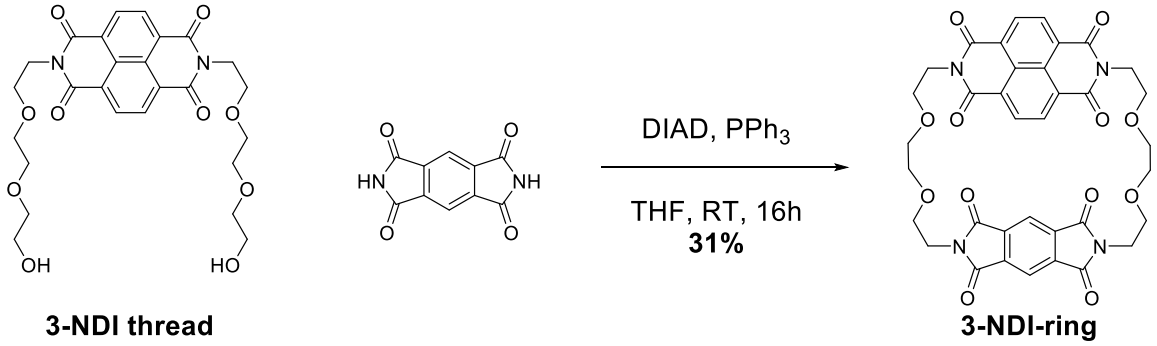

3-NDI thread **3-NDI-ring**

3-NDI-ring. 3-NDI-thread: (169 mg, 0.35 mmol, 1 eq), pyromellitic diimide (74 mg, 0.34 mmol, 1 eq) and PPh_3 (211 mg, 0.80 mmol, 2.3 eq) were suspended in dried THF (50 mL). After stirring for 30 minutes at room temperature, DIAD (160 μL, 0.81 mmol, 2.3 eq) was added and a grey precipitate was observed. The mixture was stirred for 16 hours at room temperature. The mixture was filtered and washed with DCM. The organic solvents were removed and the yellow powder was purified by column chromatography (DCM:MeOH, 19:1 v/v). After removal of solvents by rotary evaporation an off-white solid was obtained as a mixture of **3-NDI-ring** and $OPPh_3$ (**3-NDI-ring** and $OPPh_3$ co-elute from column). To remove $OPPh_3$ the off-white solid was washed 2 times with EtOH (30 mL). After drying the solid residue, an off-white powder was obtained (77 mg, 31% yield). mp: 201.1; ^{1}H NMR; (400 MHz, $CDCl_3$) δ 8.78 (s, 4H), 7.47 (s, 2H), 4.42 (t, *J* = 5.5 Hz, 4H), 3.81 (t, *J* = 5.3 Hz, 8H), 3.69 – 3.65 (m, 8H), 3.65 – 3.60 (m, 4H); ^{13}C NMR (126 MHz, CD_2Cl_2) δ 165.59, 162.68, 136.80, 130.88, 126.51, 117.31, 70.95, 70.59, 68.11, 67.89, 53.84, 53.62, 53.41, 53.41, 53.19, 52.98,

39.81, 38.21; FD–MS (MeCN) *m/z*: calculated for $C_{36}H_{30}N_4O_{12}$ [M^+]: 710.1860. Found 710.1862; FT–IR: 2919, 2870, 1717, 1667, 1456, 1390, 1337, 1246, 1099, 1045, 768, 730.

Binding study: In order to determine K_a of the **3-NDI-ring** to **DNP-thread**, a solution of **3-NDI-ring** was kept at a constant concentration (45 μM) and was titrated with an increasing concentration of **DNP-thread** in valeronitrile:MeCN, 15:85 v/v inside a cuvette of 10 mm path length. After every addition of **DNP-thread** a UV–Vis spectrum was recorded. The absorption increase at 460 nm was fitted to a 1:1 host–guest model using a Matlab script.[3]

S1.3. NMR Characterization

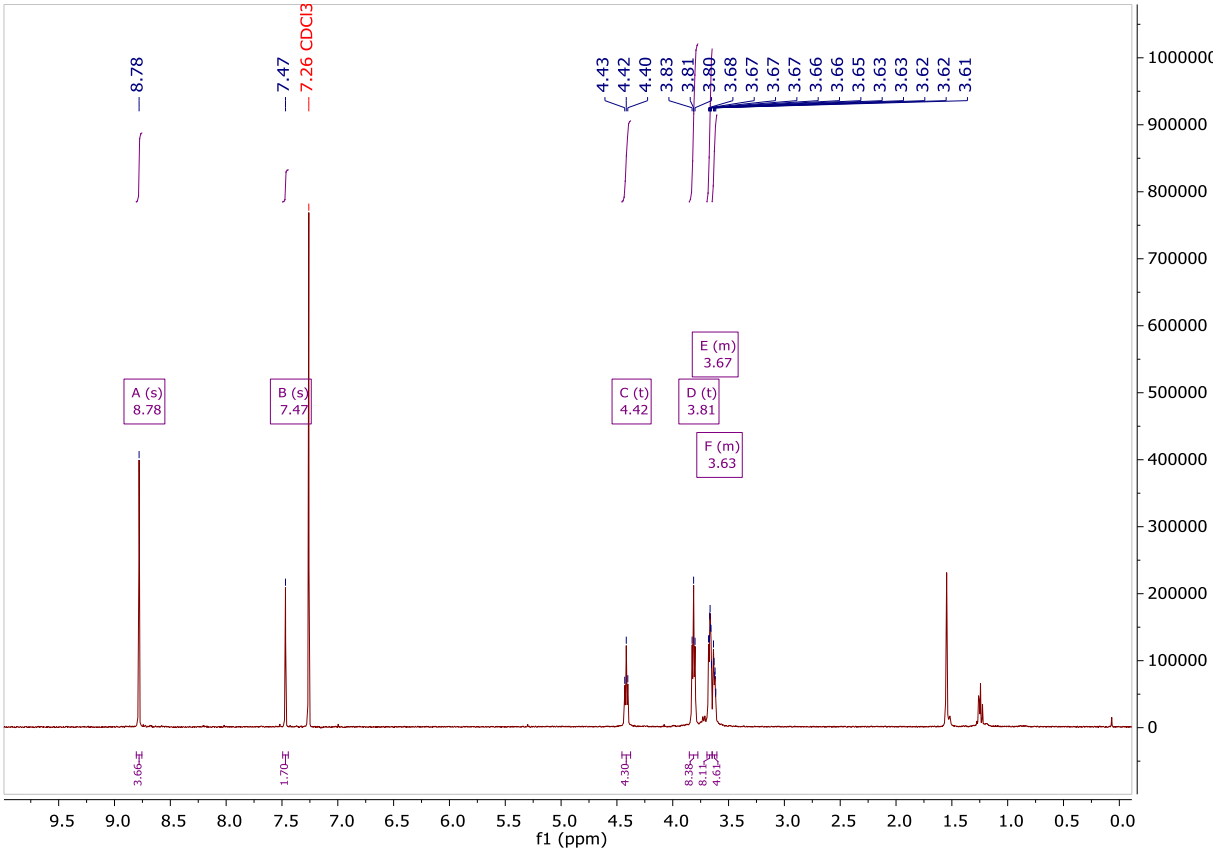

*Figure S1. [1]H NMR spectrum of final product **3-NDI-ring** (400 MHz, 298 K) in $CDCl_3$.*

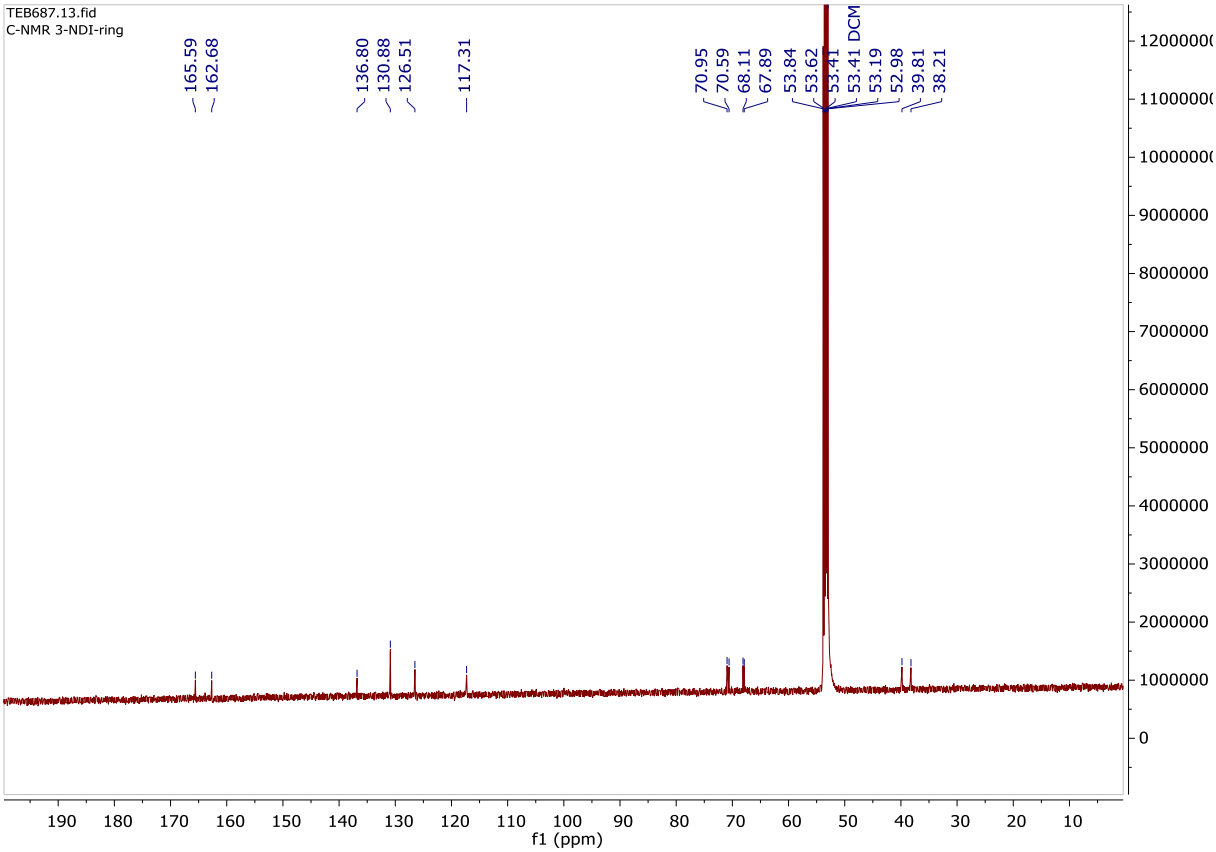

*Figure S2. ^{13}C NMR spectrum of final product **3-NDI-ring** (500 MHz, 298 K) in CD_2Cl_2.*

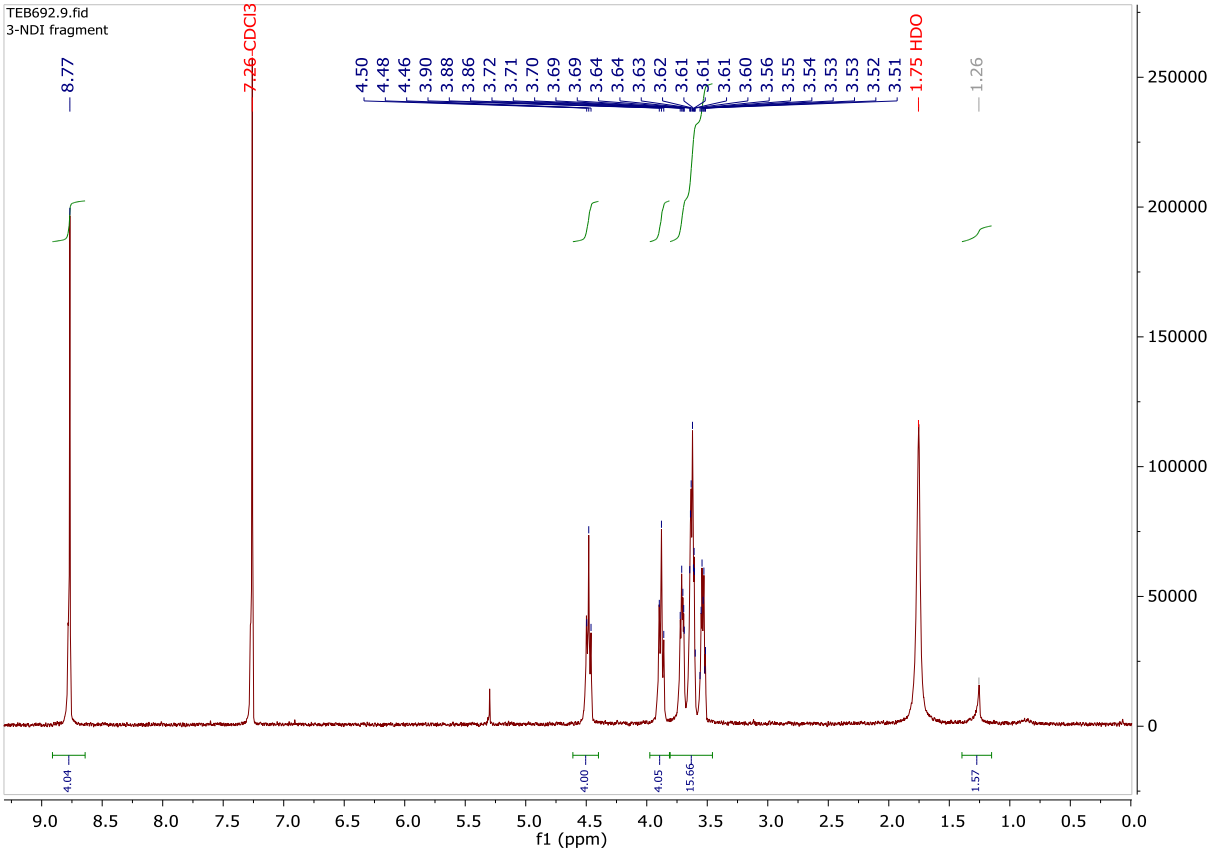

*Figure S3. [1]H NMR spectrum of **3-NDI-thread** (300 MHz, 298 K) in $CDCl_3$.*

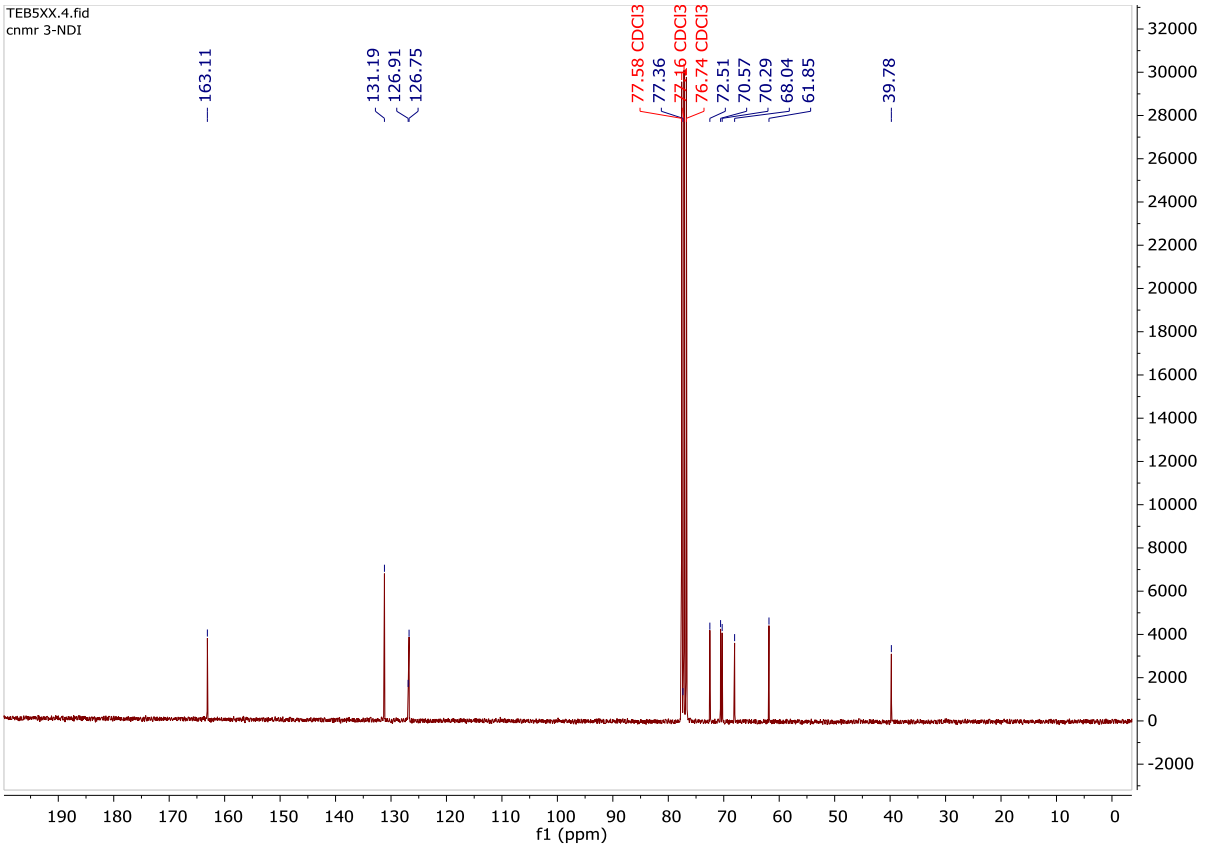

*Figure S4. [13]C NMR spectrum of **3-NDI-thread** (300 MHz, 298 K) in $CDCl_3$.*

Pseudorotaxane characterization NMR

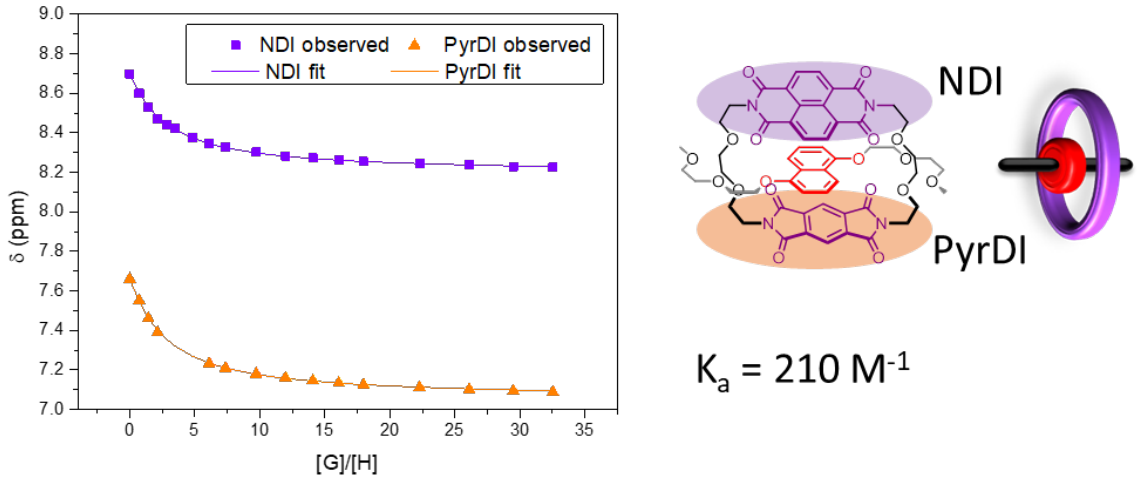

Figure S5. The titration based on Supplementary Figure 6 was used to determine the association constant K_a.

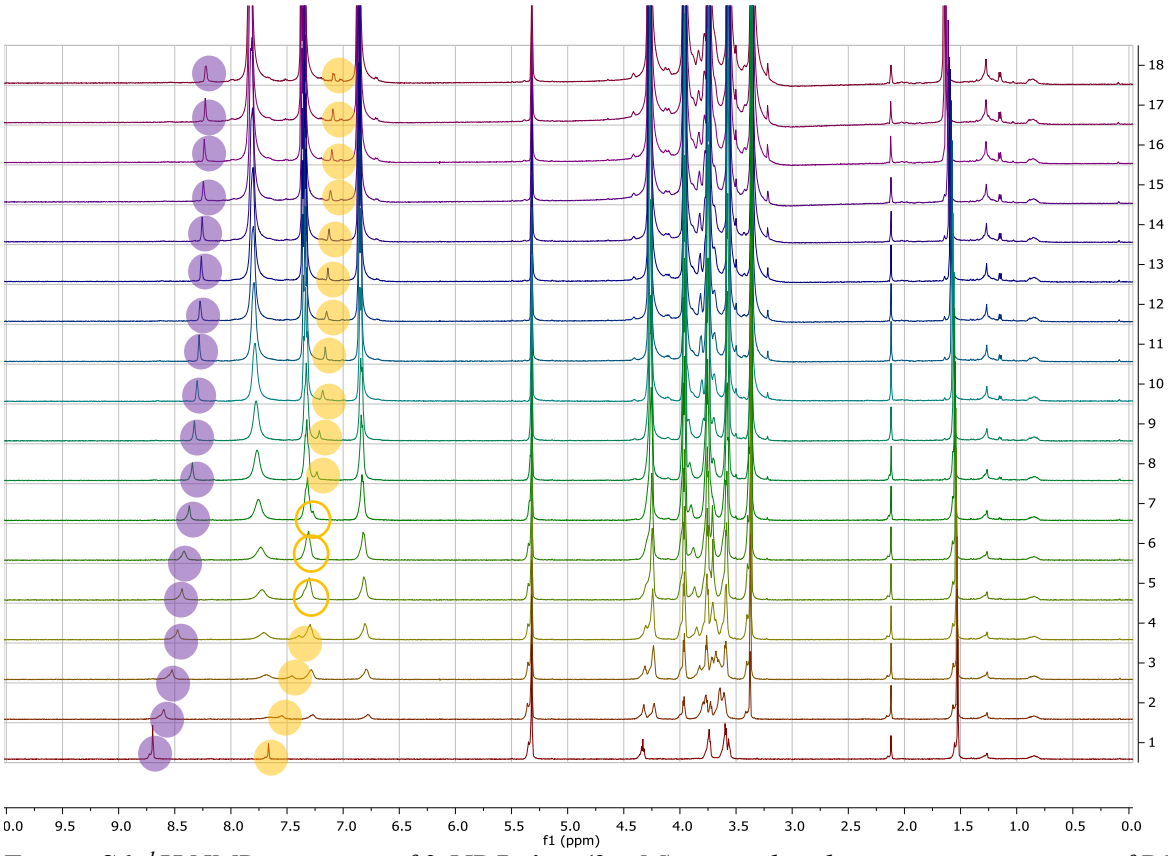

F*igure S6. ^{1}H NMR spectrum of **3-NDI-ring** (2 mM) titrated with increasing amounts of **DNP-thread** (175 mM) (500 MHz, 298 K) in CD_2Cl_2. Both aromatic signals of the **3-NDI-ring** at 8.68 ppm (Naphthalene ring, purple) and 7.65 ppm (benzene ring, yellow) show an upfield shift upon pseudorotaxane formation.*

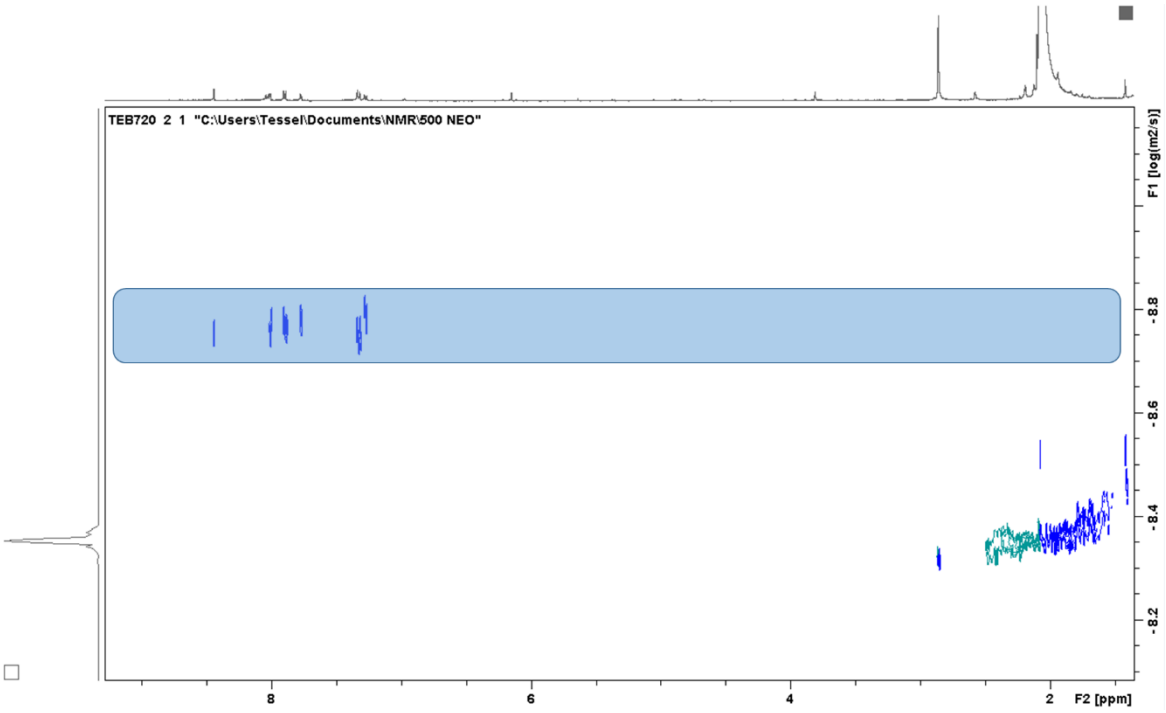

*Figure S7. DOSY ^{1}H NMR spectrum of **P1** dye (2 mM in Acetone-D_6).*

*Table S1. Hydrodynamic radius determined from DOSY ^{1}H NMR (2 mM in Acetone-D_6) for **P**$_{STATION}$ and **P1** dye.*

	P$_{STATION}$[4]	**P1**
-LogD	8.99	8.90
D (m^2 s^{-1})	1.02E-9	1.74E-9
Radius (nm)	0.7	0.39

S1.4. Optoelectronic Characterization

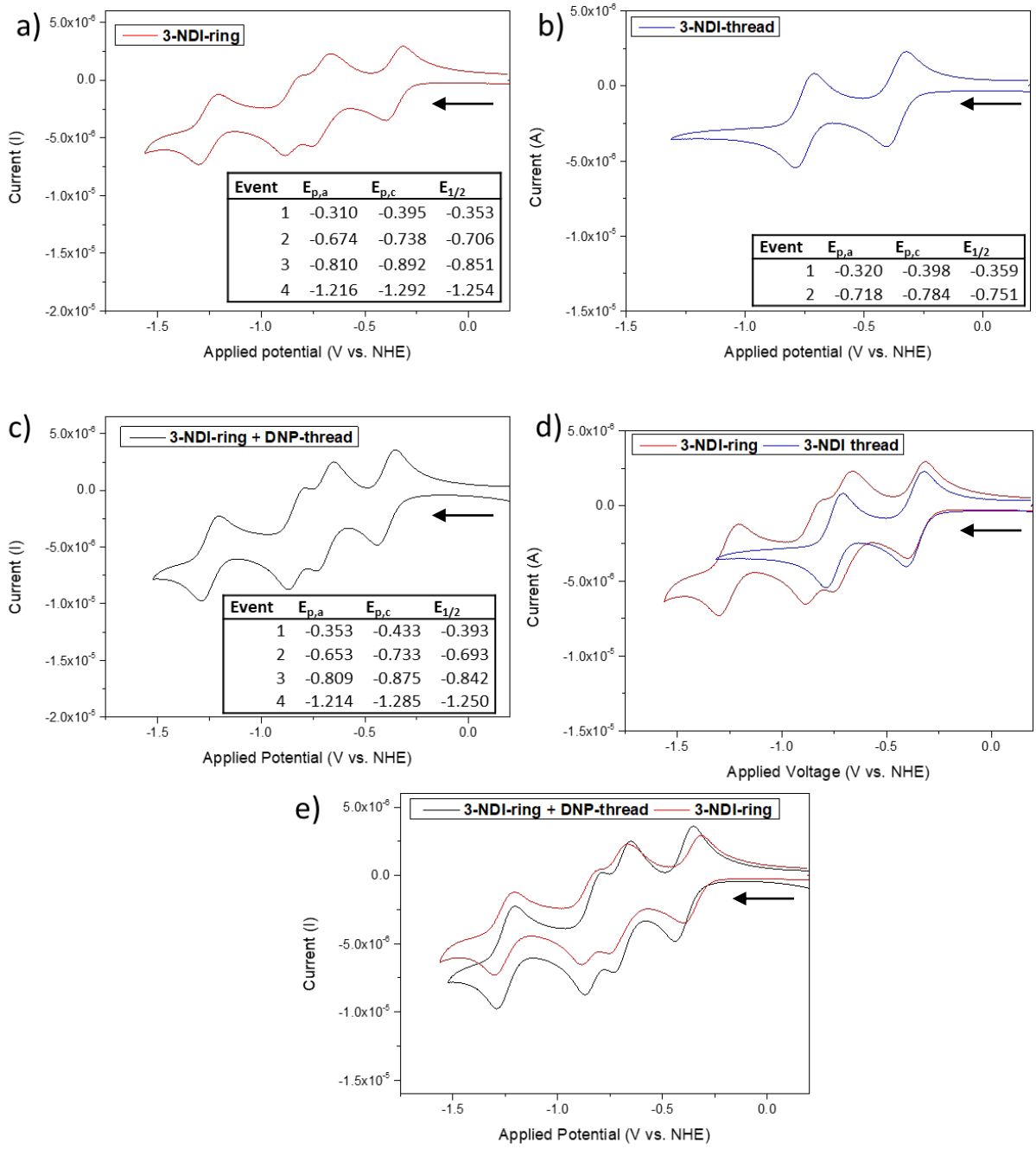

Figure S8. Cyclic voltammograms of compounds used in this study start from 0.2 V upper limit at 0.8 V and lower limit at -1.6 V vs. NHE and scan rate 0.1 V s^{-1} in 0.1 M $TBAPF_6$ in DCM using glassy carbon as working electrode, leakless Ag/AgCl as reference electrode and Pt-wire as counter electrode. The arrow indicates the scan direction. a) ***3-NDI-ring*** *(0.5 mM). b)* ***3-NDI-thread*** *(0.5 mM). c)* ***3-NDI-ring*** *(0.5 mM) in presence of* ***DNP-thread*** *(175 mM). d) Overlay of* ***3-NDI-ring*** *(0.5 mM) in presence of* ***DNP-thread*** *(175 mM) (black) and* ***3-NDI-ring*** *(0.5 mM) in absence of the* ***DNP-thread.*** *e) Overlay of* ***3-NDI-ring*** *(0.5 mM) (red) with* ***3-NDI thread*** *(0.5 mM) (blue).*

*Table S2: Redox events of **3-NDI- ring** and **3-NDI- ring + DNP-thread** vs. NHE and the potential difference of redox events in absence and in presence of the **DNP-thread** indicating the negative shift of the first redox event while the other three events do not show a negative shift.*

Event	**$E_{1/2}$ (3-NDI- ring)**	**$E_{1/2}$ (3-NDI- ring + DNP-thread)**	**$\Delta E_{1/2}$**
1	-0.393	-0.353	-0.0404
2	-0.693	-0.706	0.0128
3	-0.842	-0.851	0.0089
4	-1.250	-1.254	0.0045

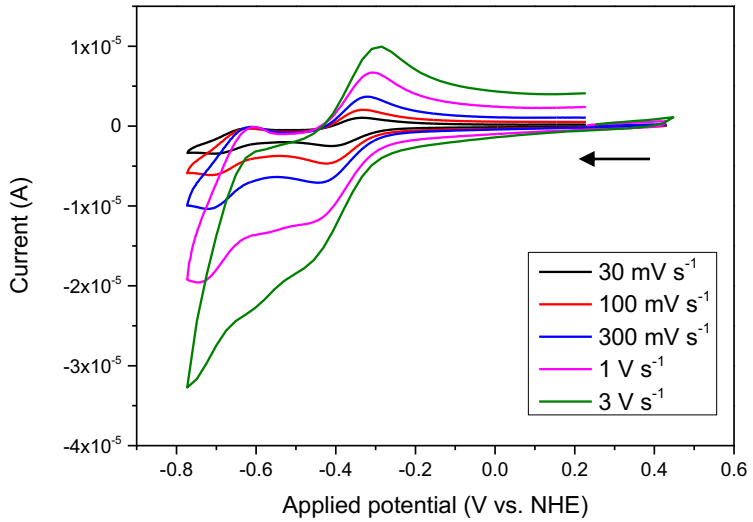

Figure S9. Overlay of cyclic voltammograms vs. NHE at different scan rates showing the irreversibility of the first reduction wave at high scan rates which is not observed for low scan rates, typical for the switching process.[5] The arrow indicates the scan direction.

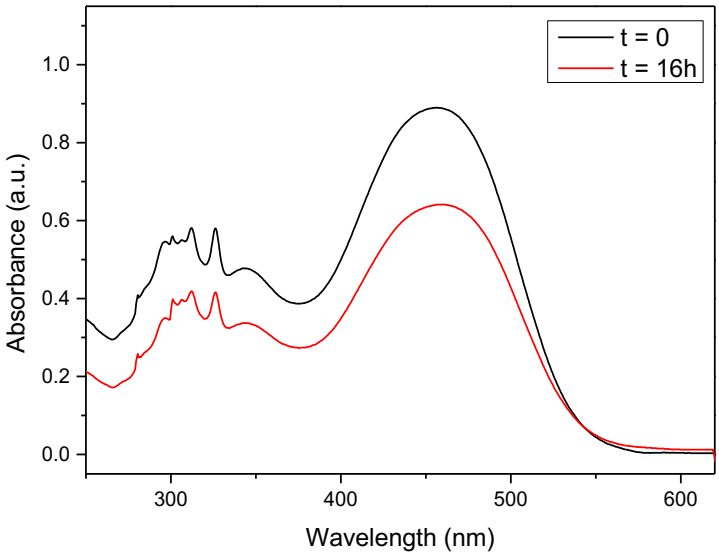

Figure S10. ***P*STATION** *Dye loading experiment showing the decrease in* ***P*STATION** *after 16h starting at t=0, 20 µM, 1.5 mL. This difference in absorption corresponds to 4.50 × 10^{-8} mol cm^{-2}* ***P*STATION** *on NiO.*

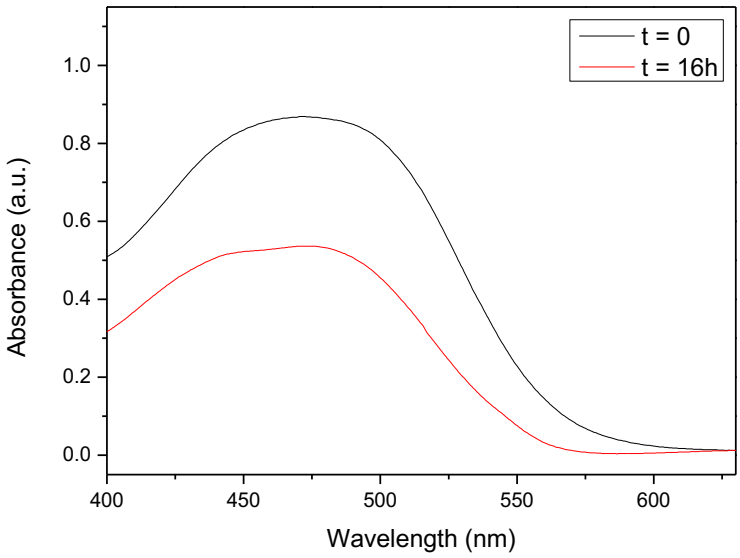

Figure S11. ***P1*** *Dye loading experiment showing the decrease in* ***P1*** *after 16h starting at t=0 20 µM, 1.5 mL. Difference in absorption corresponds to 7.03×10^{-8} mol cm^{-2}* ***P1*** *on NiO.*

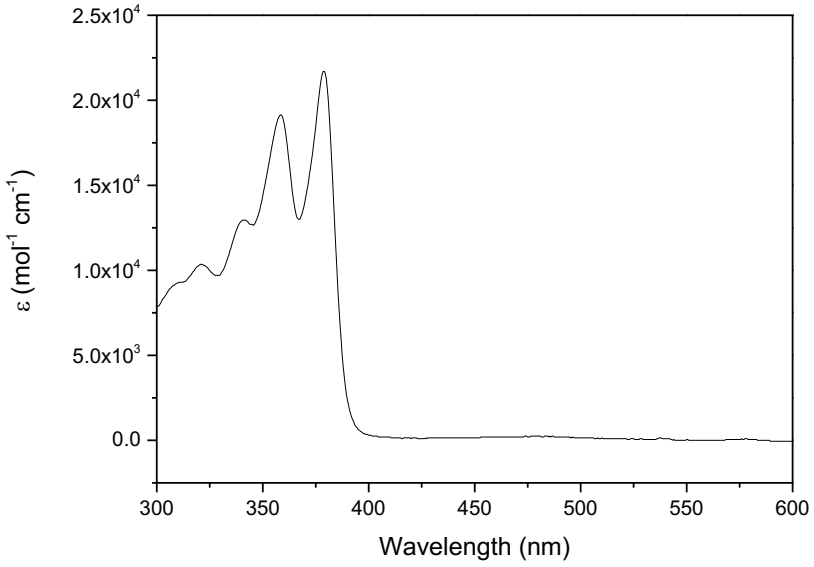

*Figure S12. UV–vis spectrum of **3-NDI-ring** in MeCN (20 µM).*

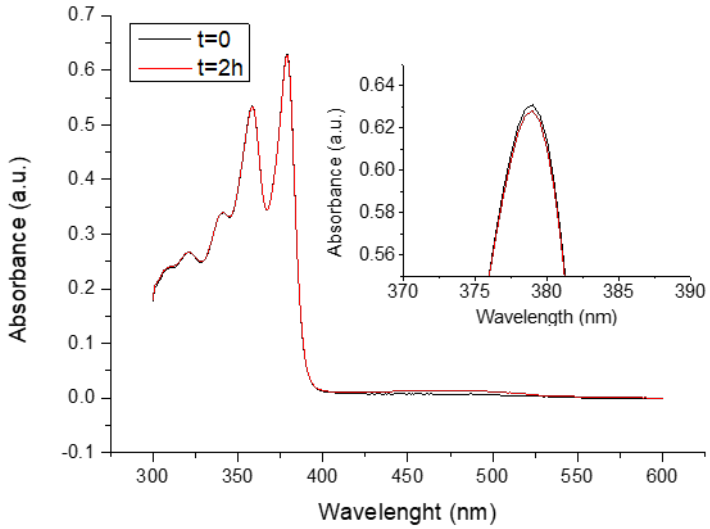

*Figure S13. **3-NDI-ring** binding to the **P**$_{STATION}$ dye adsorbed onto NiO showing the decrease in **3-NDI ring** after 2h (initial [**3-NDI-ring**] = 20 uM, 1.5mL) starting at 20 µM 1.5 mL. ΔA = 0.003 translating into a decrease of 138 nM 0.21 pmol and 1.1 nmol cm^{-2}. This means that 2.4% of **P**$_{STATION}$ dye on NiO has bound a **3-NDI-ring** molecule at 20 uM*

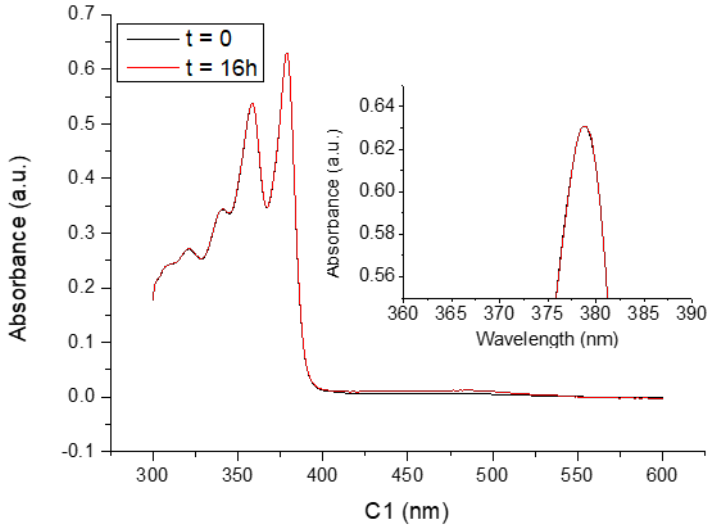

*Figure S14. Control experiment of **3-NDI ring** with **P1** dye adsorbed onto NiO showing no difference in **3-NDI ring** concentration after 2h (initial [**3-NDI-ring**] = 20 uM, 1.5mL).*

S2. Device fabrication and characterization

S2.1. Device fabrication details

FTO glass plate cleaning: FTO Glass (100 mm × 100 mm) is scrubbed with scrubbing powder and rinsed with demineralized water. Then the glass is rinsed with acetone, toluene and EtOH while dried in between every solvent. After the plates are air dried the glass is rinsed with Milli-Q water and sonicated with Deconex in Milli-Q for 30 minutes. This is followed by sonicating in Milli-Q for 30 minutes and finished by 30 minutes sonicating in EtOH. After air drying the plates were activated in a UV–ozone photoreactor before further treatment.

Working electrode: First the 100 mm × 100 mm FTO plates were cut in 4 pieces of 50 mm × 50 mm. The NiO blocking layer was installed by electrodepositing $Ni(OAc)_2$ 4•H_2O (0.13 M in Milli-Q) for 120 s at 1.1 V vs. Ag/AgCl and Pt wafer on Ti as counter electrode. A thin grey layer is visible after electrodeposition. The plates are rinsed with Milli-Q and are annealed at 300°C with a 15°C min^{-1} ramp. The plates were directly removed from the oven after 60 minutes and cooled down on a 120°C hot plate to prevent cracking of the glass. The grey color disappeared after annealing. After cooling to room temperature these plates are used for screen printing 2 layers NiO paste (mesh 77.55 fibers $inch^{-2}$, 2 × 4, 0.196 cm^2 spots on 50 mm × 50 mm plate). In between printing the layers, the plates were put on a 120°C hot plate for 10 minutes. The NiO paste is sintered using an elaborate program reported by Wood and co-workers and is summarized in Supplementary Table 3.[6] Immediately after the sintering program is finished the grey NiO plates are taken out of the hot oven and placed on a 180°C hotplate to prevent cracking. After 10 minutes the plates are cut in individual working electrode plates (12.5 mm × 25 mm). These plates were dipped in dye solution **P1** or $\mathbf{P_{STATION}}$ (0.3 mM in MeCN). After 16 hours the plates are taken out of the solution and rinsed with MeCN to remove non-adsorbed dye. The plates changed color red for **P1** and orange for $\mathbf{P_{STATION}}$. After air drying the plates are used for device assembly.

Table S3. Sintering program applied for annealing NiO working electrodes.

Segment	Start Temp. (°C)	End Temp. (°C)	Temp. ramp (°C min^{-1})	Time Ramp (min)	Time at fixed Temp.(min)
1	RT	110	3	30	30
2	110	250	2.3	60	30
3	250	340	6	15	5
4	340	400	2	30	30

NiO paste: A mixture of NiO (7.00 g) (Inframat, 20 nm), ethanol (41.55 g) (Uvasol), acetic acid (0.40 g) and of Yttrium stabilized zirconium beads (80.07 g) were ball milled for 2 hours at 1100 rpm using a DECO-PBM-V-0.4L planetary ball mill. This mixture was then added to a 250 ml beaker equipped with a large magnetic stirrer, of α-terpineol (40.16 g), of 5% ethyl cellulose (41.95 g) (50 wt% 7-15 mPa #46070, 50 wt% 30–70mPa #46080) in ethanol. The resulting mixture was stirred for 5 minutes after which it was decanted into a round bottom flask (~ 200 mL). The mixture was then reduced in volume by rotary evaporation (40ºC @ 120 mbar) to obtain a homogeneous printable paste. The paste was sonicated for 10 minutes and rested for 30 minutes prior to screen printing.

Iodide/Triiodide DSSCs

Pt Counter Electrode: Pt counter electrodes were prepared from cleaned FTO plates with predrilled holes (0.4 mm diameter) that were 12.5 mm apart so every final counter electrode (12.5 mm × 25 mm) contains one hole for vacuum backfilling of the electrolyte. The 100 mm × 100 mm FTO plates were cut in 25 mm × 50 mm sections. These plates were sonicated in HCl (0.83 mL, 37%) in EtOH (100 mL) for 30 minutes. The plates were rinsed with EtOH and air dried. Pt was electrodeposited on the FTO as working electrode with a Pt wafer on Ti counter electrode and a leakless Ag/AgCl reference electrode by applying 25 mA for 30 seconds. Electrodeposition took place in a solution containing $PtCl_4$ (0.049 g, 10 mM) in a HCl solution (0.05 M, 15 mL) with 3-(2-aminoethylamino)propyl-methyldimethoxysilane (1.5 µL). The electrodes colored equally dark grey and were rinsed with Milli-Q and EtOH. After air drying the electrodes were cut in 12.5 mm × 25 mm and used for device assembly within 24 hours.

Iodide/Triiodide Electrolyte preparation: LiI (138. mg; 1 mmol) and I_2 (25 mg, 0.1 mmol) were dissolved in 1 mL dry MeCN (Sigma-Aldrich) to obtain a 1 M electrolyte solution. The electrolyte was prepared fresh and used within 2 hours.

To prepare the 25 mM iodide/triiodide electrolyte 25 µL was added 0.9975 mL LiTFSI solution (1 M) in MeCN.

Iodide/Triiodide Device assembly: The sandwich cells were prepared by melting the one-hole Pt counter electrode to the working electrode using Meltonix polymer 1170-60 (Solaronix, Switzerland, 60 µm) with a 350 °C heating source. The ends were coated with silver paste and left to dry for 30 minutes. Then the electrolyte was introduced by vacuum back filling. After cleaning and wiping the outside the hole was sealed with the Meltonix polymer 1170-60 and a glass cover slip. The cells were directly measured after fabrication.

3-NDI-ring *DSSCs*

PEDOT Counter Electrodes: PEDOT counter electrodes were prepared from cleaned FTO plates (100 mm × 100 mm) with two predrilled holes (0.4 mm diameter, distance 7 mm) per 12.5 mm so every final counter electrode (12.5 mm × 25 mm) contains two holes for introducing the electrolyte. The 100 mm × 100 mm FTO plates were cut in 25 mm × 50 mm sections. These plates were sonicated in HCl (0.83 mL, 37%) in 100 mL EtOH for 30 minutes. The plates were rinsed with EtOH and air dried. Poly-3,4-ethylenedioxythiophene (PEDOT) was electrodeposited on the FTO as working electrode with a Pt waver on Ti counter electrode and a leakless Ag/AgCl reference electrode by performing 30 cycles of cyclic voltammetry from 0.2–1.2 V versus Ag/AgCl. The solution contained 3,4-ethylenedioxythiophene (EDOT, 2 mM), sodium dodecyl sulfate (SDS, 10 mM), and lithium perchlorate ($LiClO_4$, 10 mM). The electrodes colored equally deep blue and were rinsed with Milli-Q and EtOH. The solution was changed with a fresh solution after every deposition. After air drying the electrodes were cut in 12.5 mm × 25 mm and used for device assembly within 36 hours.

3-NDI-ring electrolyte preparation: The electrolyte was prepared in a nitrogen filled glove box. To obtain the 25 mM 50:50 **3-NDI-ring/3-NDI-ring$^{\bullet-}$** redox couple a Cobaltocene solution (0.5 mL, 12.5 mM in 1 M LiTFSI (valeronitrile:MeCN, 15:85 v/v) was added to 8.9 mg **3-NDI-ring**. The dark purple solution was stirred for 5 minutes and then led to set for 2

minutes to make sure that the oxidized Cobaltocene^{+} precipitated. The electrolyte solution was prepared freshly for every new set of DSSCs and used within 2 hours.

3-NDI-ring device assembly: The sandwich cells were prepared by melting the one-hole Pt counter electrode to the working electrode using Meltonix polymer 1170-60 (Solaronix, Switzerland) of 60 μm thickness with a 350 °C heating source. The ends were coated with silver paste and led to dry for 30 minutes. Then the electrolyte was introduced inside the glove box with a syringe. After cleaning and wiping the outside the hole was sealed with the Meltonix polymer 1170-60 and a glass cover slip. The cells were directly measured after fabrication.

S2.2. Device Characterization details

***J–V* characterization:** Dye-sensitized solar cells (DSSCs) were characterized with *J–V* curves using the Oriel LCS-100 solar simulator. The light intensity was set to 100 mW cm^{-2} with a calibrated DSSCs (Newport, 91150-2000). The current-voltage characteristics of the DSSCs were measured by applying an external potential bias and measuring the generated current with a potentiostat PGSTAT302N from Autolab with a 5 mV s^{-1} scan rate. Characterization was done at room temperature (20°C) under ambient conditions.

IPCE: IPCE was measured with the Zahner Tunable Optical Light Source TLS03 starting from 414–723 nm (resolution = 1 nm) in continuous mode with phase at 0.1 Hz and 5 counts. Characterization was performed at ambient temperature (20°C).

Electrical Impedance spectroscopy*:* Electrical impedance spectroscopic (EIS) measurements were performed with the Zahner LSW-1 light source controlled by Zahner PP211 potentiostat. The measurements were performed at different light intensities (60, 50, 45, 40, 30, 20, 10 and 5 mW cm^{-2}) from 1–100 KHz to lower limit 0.1 Hz at an amplitude of 5 mV. Characterization was done at ambient temperature (20°C).

Chopped light voltammetry*:* Chopped light voltammetry was performed with the Zahner LSW-1 light source controlled by Zahner PP211 potentiostat. The light source intensity was programmed to perform on/off cycles of 10 seconds while every cycle the light intensity was increased with 5 mW cm^{-2} starting from 5 mW cm^{-2}.and ending at 50 mW cm^{-2}. Characterization was done at room temperature (20°C).

S2.3. Device Characterization of Iodide/Triiodide DSSCs

Photovoltaic performance. To enable a fair comparison between **P1-** and **P$_{STATION}$**-based DSSCs, devices were prepared using the iodide/triiodide redox electrolyte (1 M LiI and 0.1 M I_2 in MeCN) and NiO photocathodes (3.5 μm, 0.196 cm^{-2}) prior sensitized with **P1** or **P$_{STATION}$** MeCN solution for 16 hours. Measurement of dye loading by dye uptake experiments revealed that the surface coverage of **P1** (Γ=7.03× 10^{-8} mol cm^{-2}) is approximately 50% higher that of **P$_{STATION}$** (Γ= **P$_{STATION}$** 4.50 × 10^{-8} mol cm^{-2}). The DSSCs were assembled with Pt counter electrodes and characterized with AM 1.5G illumination (100 mW cm^{-2}). Summarized in Supplementary Table 4, **P1**/iodide DSSCs gave a PCE (0.061% ± 0.002%) comparable to the best performing analogous devices literature (0.075%),[6] The PCE of the DSSC based on **P$_{STATION}$** dye is lower (0.041% ± 0.002%) in comparison. The lower dye loading leaves more exposed NiO prone to recombination (Supplementary Figure 27) affecting the V_{OC} and J_{SC} which is also reflected in the small difference in maximum higher incident to photocurrent efficiency (IPCE) (Supplementary Figure 18, 17.7% at 500 nm for **P1** and 15.1% at 485 nm for **P$_{STATION}$**). meaning that PCE differences between **P1** and **P$_{STATION}$** can be simply rationalized by differences in surface coverage and therefore light harvesting, unsurprising given the increased molecular size of **P$_{STATION}$** upon incorporation of the **DNP** binding site (r_H = 0.68 nm for **P$_{STATION}$** versus r_H = 0.39 nm for **P1,** Supplementary Table 1). Therefore, differences in subsequent DSSCs described employing **3-NDI-ring** as redox mediator are attributable to pseudorotaxane-mediated preorganization and ring-launching effects.

Studying the photovoltaic performances of DSSCs based on **P$_{STATION}$** and **P1** and the **3-NDI-ring** electrolyte, Poly(3,4-ethylenedioxythiophene) (PEDOT) was used in place of Pt as the counter electrode given its lower charge transfer resistance for organic radical redox couples.[7] The low solubility of **3-NDI-ring** in MeCN compared to I^-/I_3^- limits DSSC to a 40 times lower redox mediator concentration. Decreased electrolyte concentration leads to lower efficiency as is also represented by comparing 25 mM iodide/triiodide DSSCs versus 1 M iodide/triiodide DSSCs showing a 10 times drop in PCE (Supplementary Table 4).

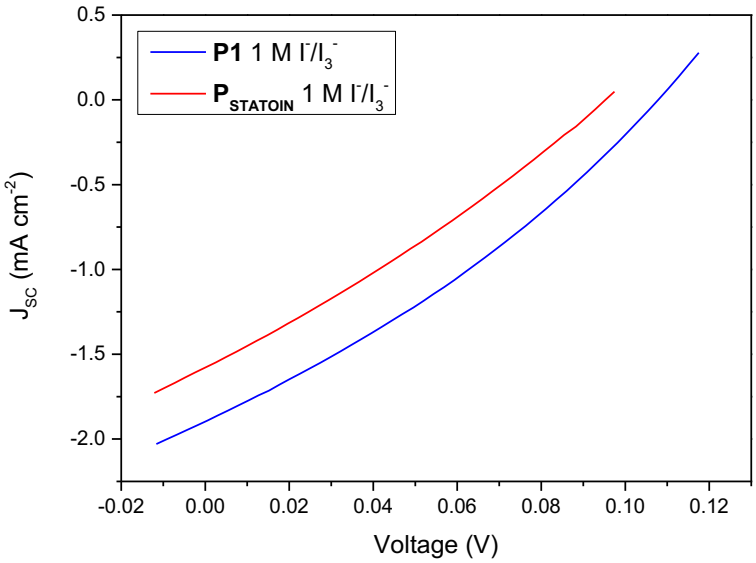

*Figure S15. J-V curves of DSSCs composed of **P1** (blue line) and **P**$_{STATION}$ (red line) under AM 1.5G illumination (100 mW cm^{-2}) with 1 M I^-/I_3^- redox couple in MeCN and Pt Counter electrode.*

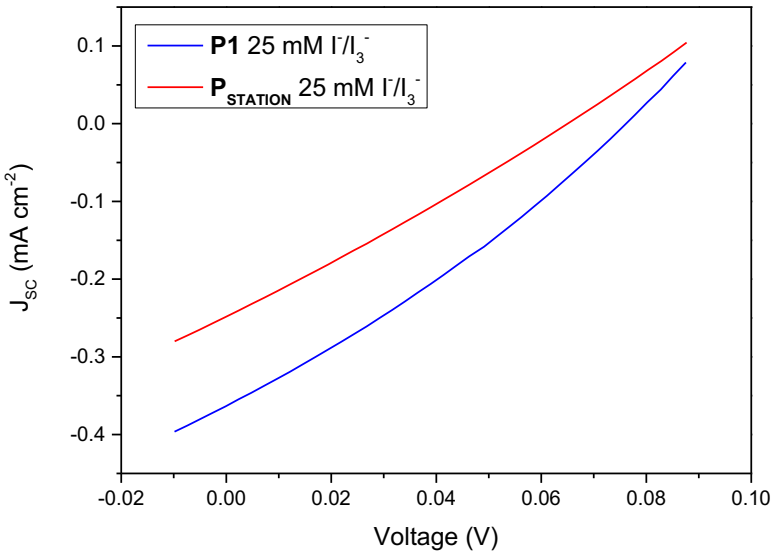

*Figure S16. J–V curves of DSSCs composed of **P1** (blue line) and **P**$_{STATION}$ (red line) under AM 1.5G illumination (100 mW cm-2) with 25 mM I^-/I_3^- redox couple in 1 M LiTFSI in MeCN and Pt Counter electrode.*

*Table S4. Summary of the photovoltaic performance data for DSSC based on **P1** and **P$_{STATION}$** under AM 1.5G illumination (100 mW cm^{-2}) with the I^-/I_3^- redox couple 1 M and 25 mM) in 1 M LiTFSI in MeCN. The average (N=5) performance is provided with the best performing cell in brackets.*

Dye	Electrolyte	V_{oc} (V)	J_{sc} (mA cm^{-2})	FF	PCE (%)
P1	1 M I^-/I_3^-	107 ± 3 (110)	1.92 ± 0.05 (1.92)	0.296 ± 0.003 (0.298)	0.061 ± 0.002 (0.063)
P$_{STATION}$	1 M I^-/I_3^-	96.1 ± 1.5 (97.4)	1.51 ± 0.1 (1.61)	0.275 ± 0.009 (0.281)	0.0409 ± 0.002 (0.0430)
P1	25 mM I^-/I_3^-	72 ± 11 (83)	0.365 ± 0.031 (0.394)	0.294 ± 0.018 (0.307)	0.0078 ± 0.0010 (0.0086)
P$_{STATION}$	25 mM I^-/I_3^-	63 ± 6 (68)	0.277 ± 0.031 (0.308)	0.266 ± 0.015 (0.271)	0.0046 ± 0.0004 (0.0051)

Chopped light 25 mM I^-/I_3^- redox couple

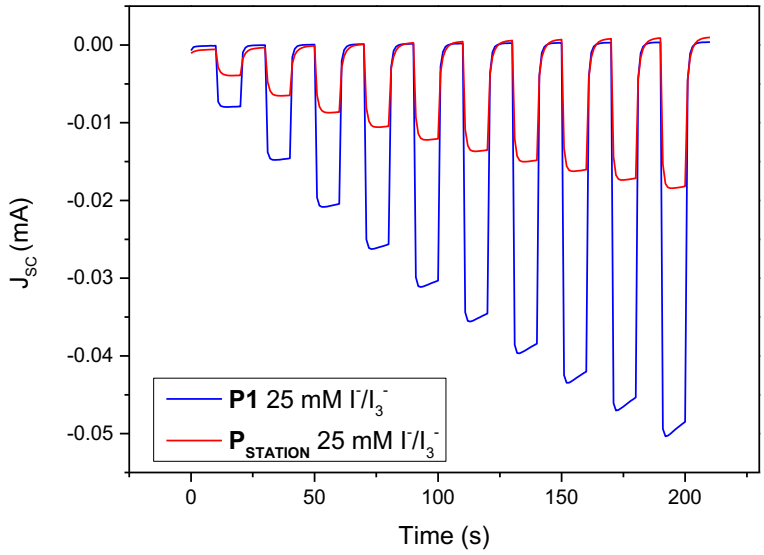

*Figure S17. Chopped light voltammetry at different light flux varying from 5 mW cm^{-2} to 50 mW cm^{-2} with on/off cycles of 10 seconds for the DSSCs composed of **P1** (blue line) and **$P_{STATION}$** (red line) with 25 mM I^-/I_3^- redox couple in 1 M LiTFSI in MeCN. The tailing behavior of the photocurrent signal response is characteristic for diffusion limitations of the redox couple.*[8]

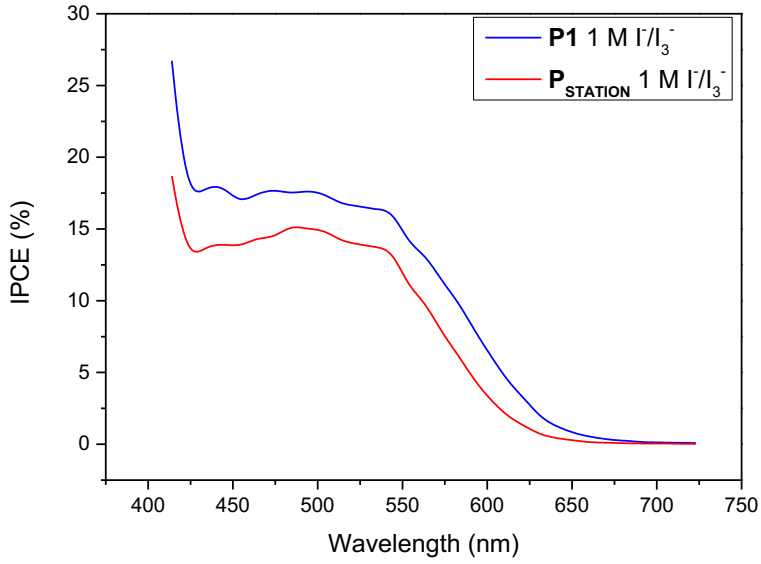

*Figure S18. A photocurrent action spectrum of the **$P_{STATION}$** based system (red) and the **P1** based system (blue) with 1 M I^-/I_3^- redox couple in MeCN.*

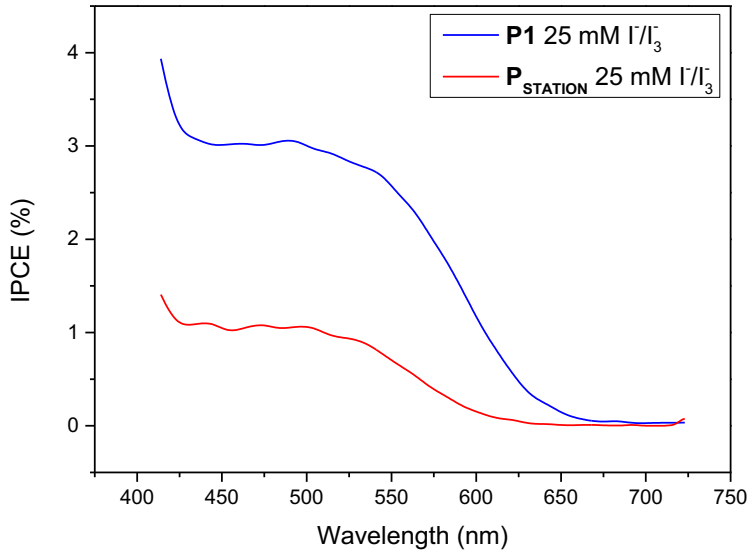

Figure S19. A photocurrent action spectrum of the ***P*****$_{STATION}$** *based system (red) and the* ***P1*** *based system (blue) with 25 mM* I^-/I_3^- *redox couple in 1 M LiTFSI in MeCN.*

2.4. Comparison IPCE set-up and solar simulator

IPCE is measured form 414–723 nm (resolution = 1 nm) in continuous mode. If we transform the IPCE spectrum of **P1** 1M iodide/triiodide DSSC (Supplementary Figure 18) to the photonflux and integrate the spectrum using a python script we can determine the photocurrent density that we can compare with the photocurrent density that we actually measure in the *J–V* curves with the solar simulator (Supplementary Figure 20) with AM 1.5G illumination (100 mW cm^{-2}). As these values for the photocurrent density are very similar, we assume that the IPCE measured for all DSSC under study match the outcome of the *J–V* curves.

Table S5. Integrated photocurrent density form IPCE measurement versus photocurrent density measured by J–V-curve with AM 1.5G illumination (100 mW cm^{-2}).

Method	**Measured photocurrent density (mA cm^{-2})**
Integrated photocurrent	2.10
J–V curve	1.97

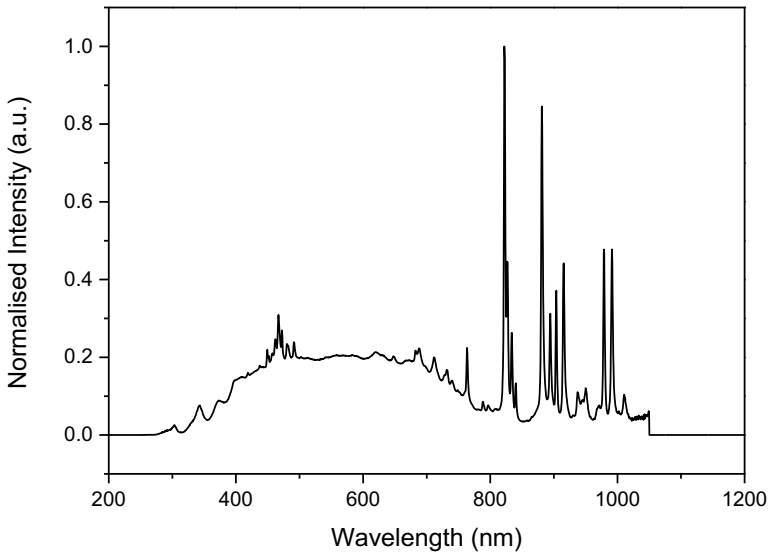

Figure S20. Spectrum solar simulator used in this study Oriel LCS-100 solar simulator.

2.5. Photovoltaic variation and statistics

*Table S6. Overview of results obtained from J–V curves under with AM 1.5G illumination (100 mW cm^{-2}) of all **3-NDI-ring** DSSCs that were prepared during this study.*

sc#	Dye	V_{OC} (V)	J_{SC} (mA cm^{-2})	FF	PCE (%)
sc0379	**P1**	0.238	-0.138	0.361	0.0118
sc0380	**P1**	0.208	-0.101	0.321	0.0067
sc0381	**P1**	0.205	-0.108	0.316	0.0070
sc0382	**P1**	0.247	-0.112	0.347	0.0096
sc0383	**P1**	0.198	-0.109	0.314	0.0068
sc0390	**P1**	0.210	-0.210	0.331	0.0146
sc0392	**P1**	0.198	-0.141	0.246	0.0069
sc0390	**P1**	0.168	-0.219	0.318	0.0117
sc0392	**P1**	0.198	-0.141	0.246	0.0069
sc0394	**P$_{STATION}$**	0.300	-0.501	0.376	0.0565
sc0395	**P$_{STATION}$**	0.385	-0.411	0.382	0.0604
sc0396	**P$_{STATION}$**	0.343	-0.429	0.342	0.0504
sc0397	**P$_{STATION}$**	0.338	-0.355	0.302	0.0363
sc0401	**P$_{STATION}$**	0.320	-0.376	0.344	0.0565
sc0497	**P$_{STATION}$**	0.326	-0.410	0.356	0.0475
sc0498	**P$_{STATION}$**	0.335	-0.399	0.341	0.0456
sc0388	**P$_{STATION}$**	0.338	-0.273	0.412	0.0380
sc0413	**P$_{STATION}$**	0.303	-0.345	0.377	0.0393

*Table S7: Statistics of all **3-NDI-ring** DSSCs under study based on Supplementary Table 6.*

Dye		V_{OC} (V)	J_{SC} (mA cm^{-2})	FF	PCE (%)
P$_{STATION}$	MEAN	0.332	-0.389	0.359	0.048
	STDEV	0.024	0.060	0.030	0.008
	Error	0.008	0.020	0.010	0.003
P1	MEAN	0.208	-0.142	0.311	0.009
	STDEV	0.022	0.042	0.020	0.003
	Error	0.007	0.014	0.007	0.001

Photovoltaic stability test:

Table S8. Photovoltaic performance of ***P*****$_{STATION}$** ***3-NDI-ring*** *(sc0394) DSSC at different points in time measured with the Zahner LSW-1 light source controlled by Zahner PP211 potentiostat (50 mW cm^{-2}). Characterization was done at ambient temperature (20°C).*

Time	V_{OC} (V)	J_{SC} (A cm^{-2})	FF	PCE (%)
0h	0.321	-0.314	0.370	0.074
2h	0.303	-0.364	0.355	0.078
5h	0.356	-0.290	0.373	0.077
24h	0.313	-0.220	0.362	0.050

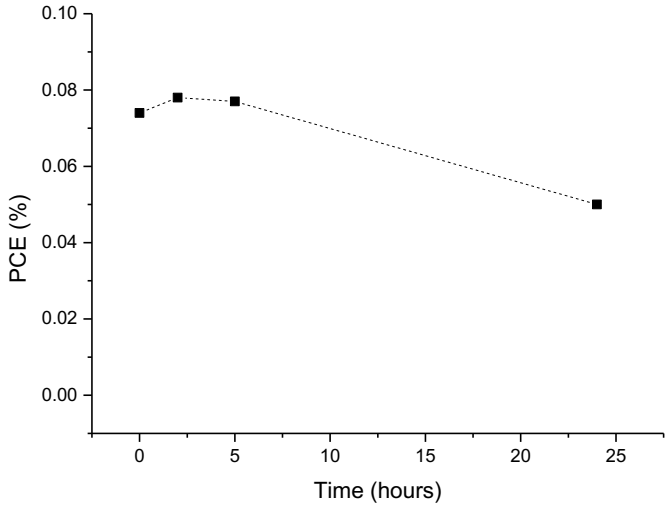

Figure S21. Short-term stability (@20°C) of ***P*****$_{STATION}$** ***3-NDI-ring*** *(sc0394) DSSC at different points in time measured with the Zahner LSW-1 light source controlled by Zahner PP211 potentiostat (50 mW cm^{-2}). In the first two hours the DSSC was illuminated with 50 mW cm^{-2} (Zahner LSW-1 light source) and then left at open circuit in the light for 24 hours. The drop in efficiency is attributed to oxygen leaking into the system.*

S2.6. Electrical Impedance Spectroscopic measurements

EIS experiments were performed with a Zahner Zennium potentiostat. All cells were measured were performed at open circuit voltage with an AC perturbation amplitude of 10 mV. The AC frequency was measured from 100 mHz to 1 KHz. The measured data were fitted with an equivalent circuit built from a Randles circuit that represents the series resistance and the and a transmission line element that represents the photoelectrode.[9] The counter electrode was not included because this signal was not observed. Using this model gives values for the chemical capacitance (C_μ) and recombination resistance (R_{REC}) at the photocathode from which the hole life time τ_h can be determined according to equation 1.

$$\tau_h = R_{REC} C_\mu \quad (1)$$

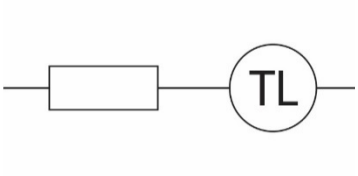

Figure S22. The equivalent circuit used to fit the impedance data based on the transmission line element.[9]

3-NDI-ring DSSCs

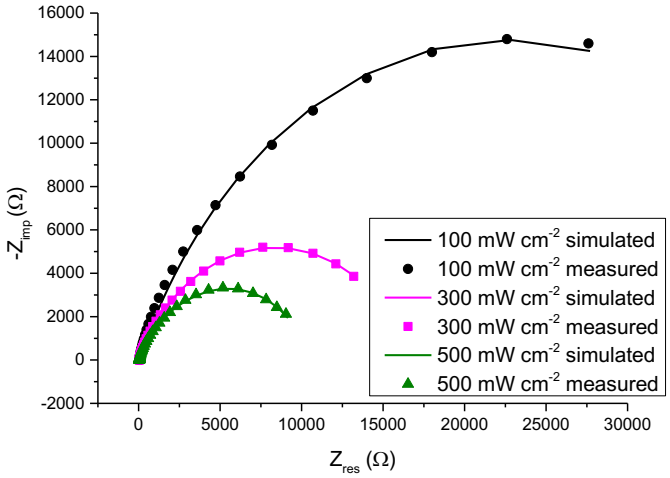

*Figure S23. Nyquist plots of the DSSCs consisting of **P1** and **3-NDI-ring** electrolyte (25 mM) in 1 M LiTFSI (valeronitrile:MeCN, 15:85 v/v) at different light intensities (50 mW cm^{-2} in green, 30 mW cm^{-2} in pink and 10 mW cm^{-2} in black) at open circuit voltage.*

*Table S9. Results for Recombination Resistance R_{REC} Chemical capacitance C_μ and Hole lifetime τ_h by fitting the obtained impedance data of the DSSCs consisting of **P1** and **3-NDI-ring** electrolyte using the model in Supplementary Figure 23 based on Fabregat-Santiago et al.[4]*

P1				
Power (W cm^{-2})	Voltage	R_{REC} ($\times 10^3$ Ohm)	C_μ ($\times 10^{-6}$ F)	τ_h (s)
600	0.205	6.69	8.68	0.058
550	0.206	9.07	8.55	0.078
500	0.202	9.03	11.8	0.107
450	0.198	0.11	9.92	0.109
400	0.193	0.12E	8.83	0.109
300	0.178	0.131	8.84	0.116
200	0.157	0.22E	8.03	0.177
100	0.118	0.45E	6.01	0.272
50	0.079	0.79E	5.14	0.407

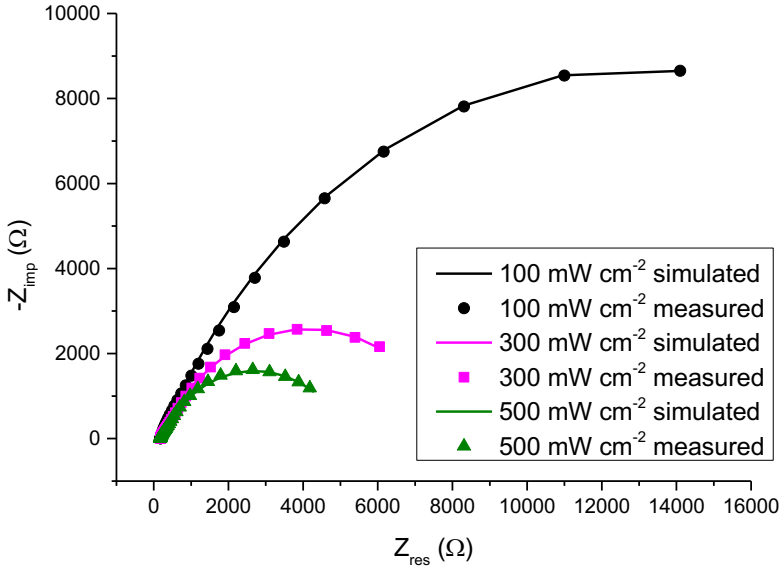

*Figure S24. Nyquist plots of the DSSCs consisting of **P$_{STATION}$** and **3-NDI-ring** electrolyte (25 mM) in 1 M LiTFSI (valeronitrile:MeCN, 15:85 v/v) at different light intensities (50 mW cm^{-2} in green, 30 mW cm^{-2} in pink and 10 mW cm^{-2} in black) at open circuit voltage.*

*Table S10. Results for Recombination Resistance R_{REC} Chemical capacitance C_μ and Hole lifetime τ_h by fitting the obtained impedance data of the DSSCs consisting of **$P_{STATION}$** and **3-NDI-ring** electrolyte using the model in Supplementary Figure 24 based on Fabregat-Santiago et al.*[9]

$P_{STATION}$				
Power	Voltage	R_{REC} ($\times 10^3$ Ohm)	C_μ ($\times 10^{-5}$ F)	τ_h (s)
500	0.277	4.04	2.59	0.104
450	0.263	5.04	4.48	0.226
400	0.258	5.36	4.72	0.253
300	0.238	7.79	2.18	0.170
200	0.21	0.11	2.73	0.287
100	0.161	0.23	1.62	0.366
50	0.117	0.52	1.05	0.544

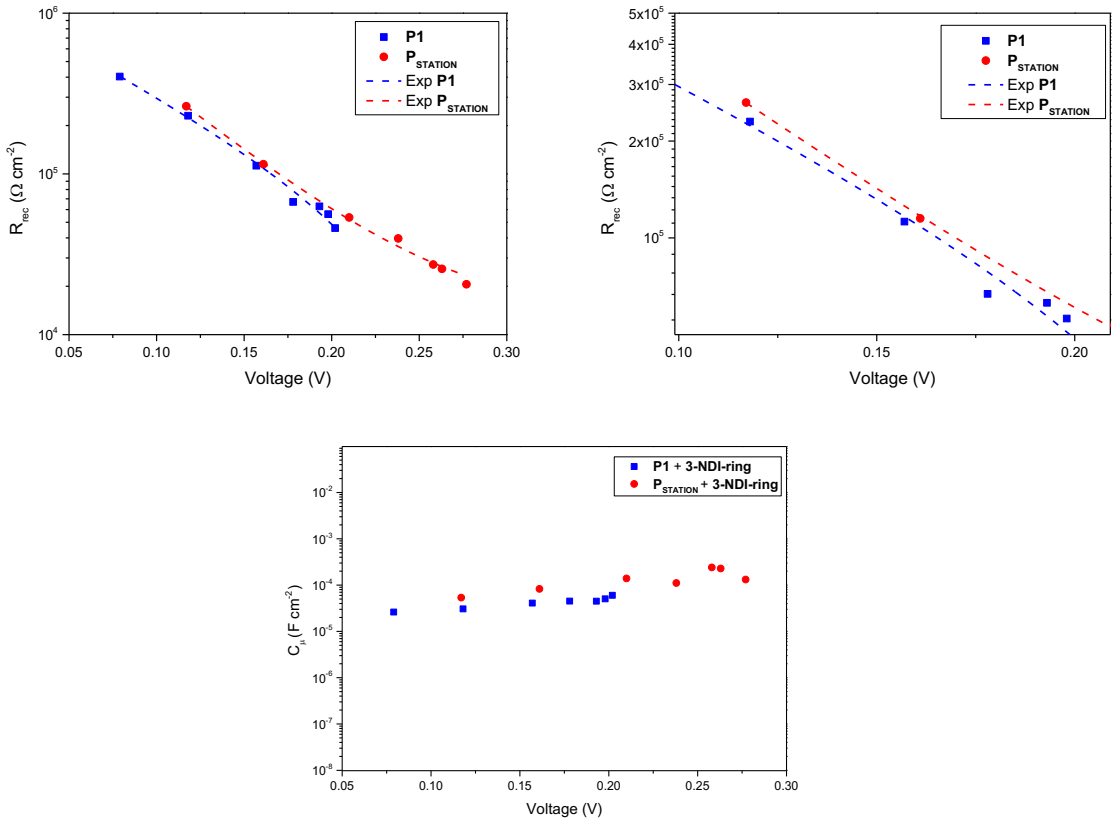

*Figure S25. R_{REC} against measured voltage (above) for **P1** (blue) and **$P_{STATION}$** (red) and C_μ against measured voltage (below) as visualization of Table S12 and Table S13.*

Supplementary Figure 25 shows the recombination resistance by fitting the obtained impedance data of the DSSCs for **P1** and **$P_{STATION}$** combined with **3-NDI-ring**. The relationship with

equation (2) between V and R_{REC} and an exponent parameter β indicating the recombination order.[10] By fitting the data points with experimental equation (2) the value of β can be calculated which can be considered as recombination order related to the device type.

$$R_{REC} = R_0 \exp\left(-\frac{q\beta}{k_B T} V\right) \quad (2)$$

As the slope of both exponential fits are almost identical (-16 for $\mathbf{P_{STATION}}$ and -17 **P1**) the value of β was found to be 0.4 in both cases. This also means that the DSSC under study exhibit the same "diode ideality factor" *m* according to equation (3).

$$m = \frac{1}{\beta} \quad (3)$$

This means that the difference in R_{REC} is directly related to the **P1** and $\mathbf{P_{STATION}}$ and are not due to a difference in "diode ideality" such as different trap states due to NiO material differences.[10,11]

1 M Iodide/Triiodide DSSCs

EIS experiments were performed with a Zahner Zennium potentiostat. All cells were measured were performed at open circuit voltage with an AC perturbation amplitude of 10 mV. The AC frequency was measured from 100 mHz to 1 KHz. The measured data were fitted with an equivalent circuit build from a Randles circuit that represents the series resistance and the counter electrode resistance and a transmission line element that represents the photoelectrode.[9]

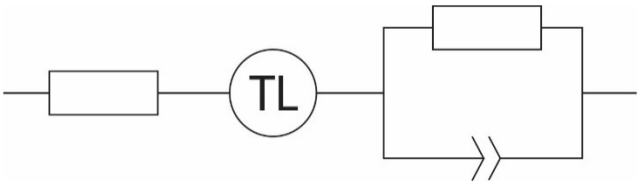

Figure S26. The equivalent circuit used to fit the impedance data based on the transmission line element.[4]

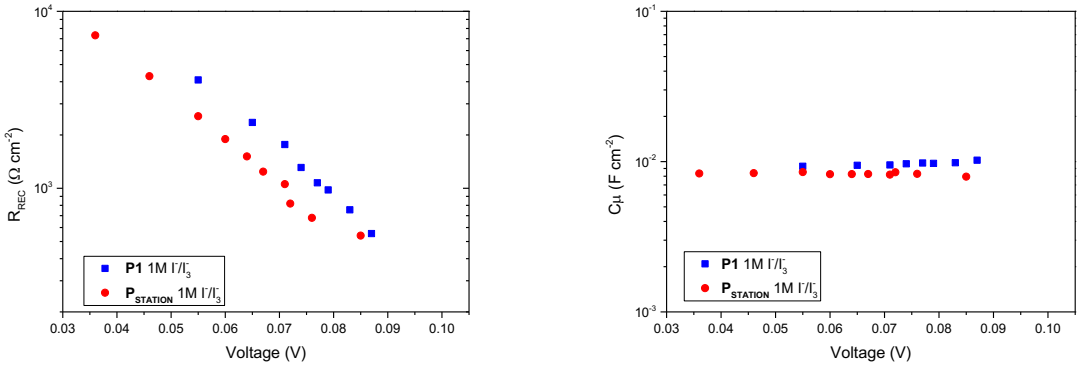

*Figure S27. R_{REC} against measured voltage (left) with 1 M iodide/triiodide electrolyte for **P1** (blue) and **$P_{STATION}$** (red) and C_μ against measured voltage (right) using the model in Supplementary Figure 26 based on Fabregat-Santiago et al.[4]*

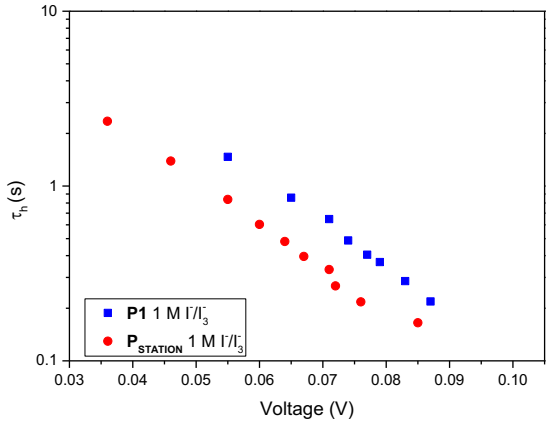

Figure S28. τ_h against measured voltage (left) with 1 M iodide/triiodide electrolyte for ***P1*** *(blue) and* ***P*** $_{STATION}$.

S2.7. SEM Characterization NiO

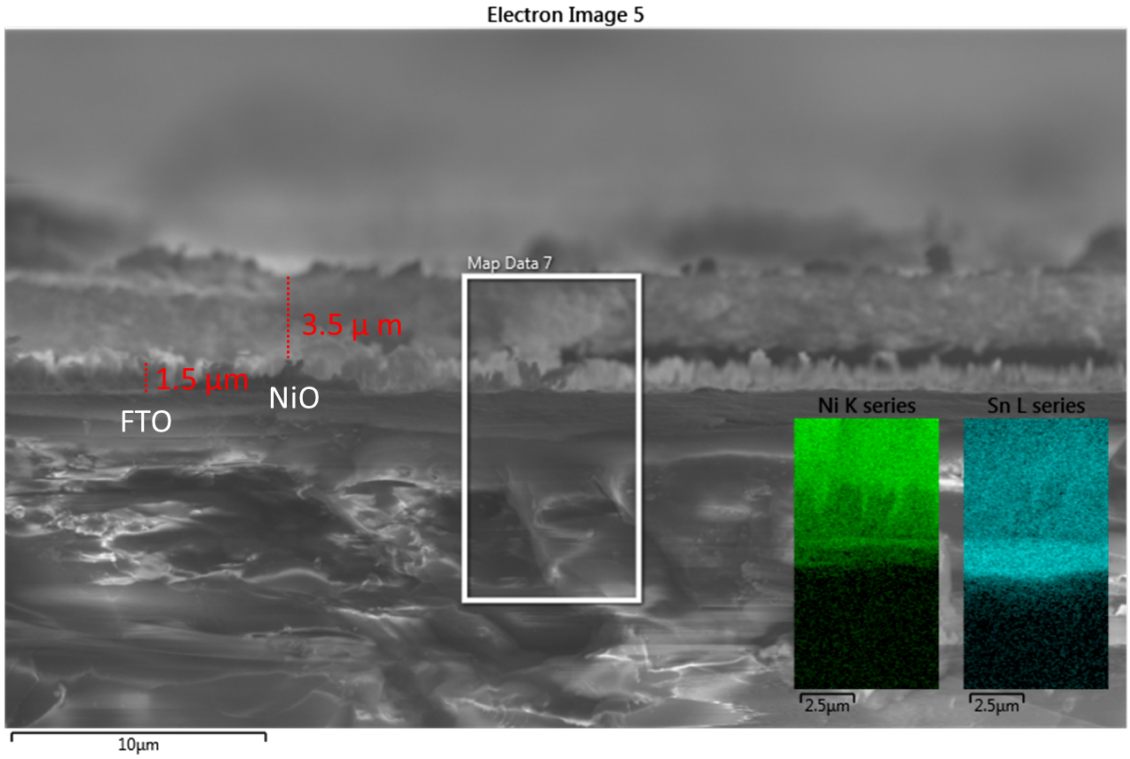

Figure S29. SEM micrograph of the cross section of NiO on FTO glass showing the layer thickness together with the energy dispersive x-ray spectrum (EDX) for Ni atoms and Sn atoms distinguishing the FTO layer and the NiO layer.

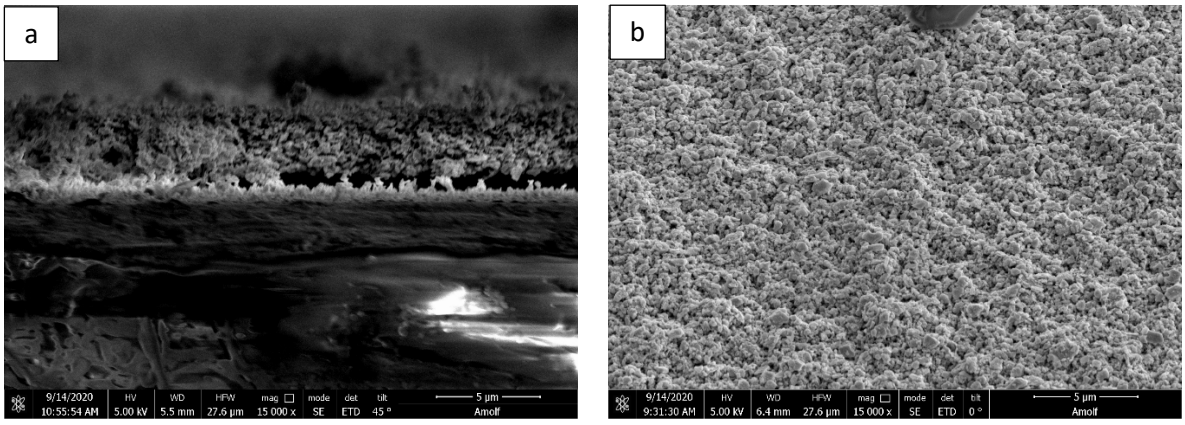

Figure S30. SEM micrograph of the a) cross section of NiO on FTO glass and b) of the surface.

S2.8. BET Characterization NiO

The porosity of the NiO nanoparticles was estimated by nitrogen absorption via Brunauer-Emmett-Teller (BET) analysis on a Thermo Scientific Surfer Analyzer. The NiO paste was applied and sintered according to the method described in Supplementary Table 3. The surface area NiO nanoparticles under study was determined to be 59.1 cm^2 g^{-1} calculated from the adsorption isotherm (Supplementary Figure 31) which corresponds to other NiO nanoparticles pastes found in literature.[12]

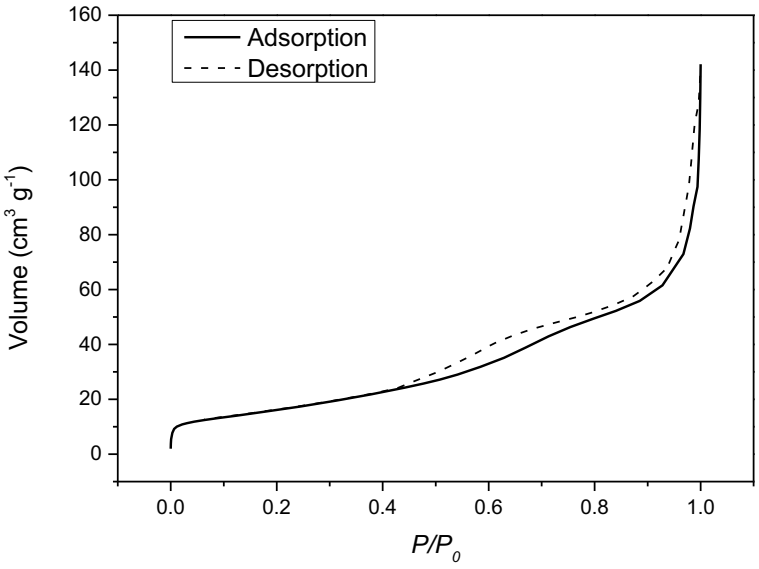

Figure S31. Adsorption and desorption isotherm of NiO nanoparticles under study. This type II isotherm is characteristic for a mesoporous material.

S2.9. Size of screen printed NiO spots

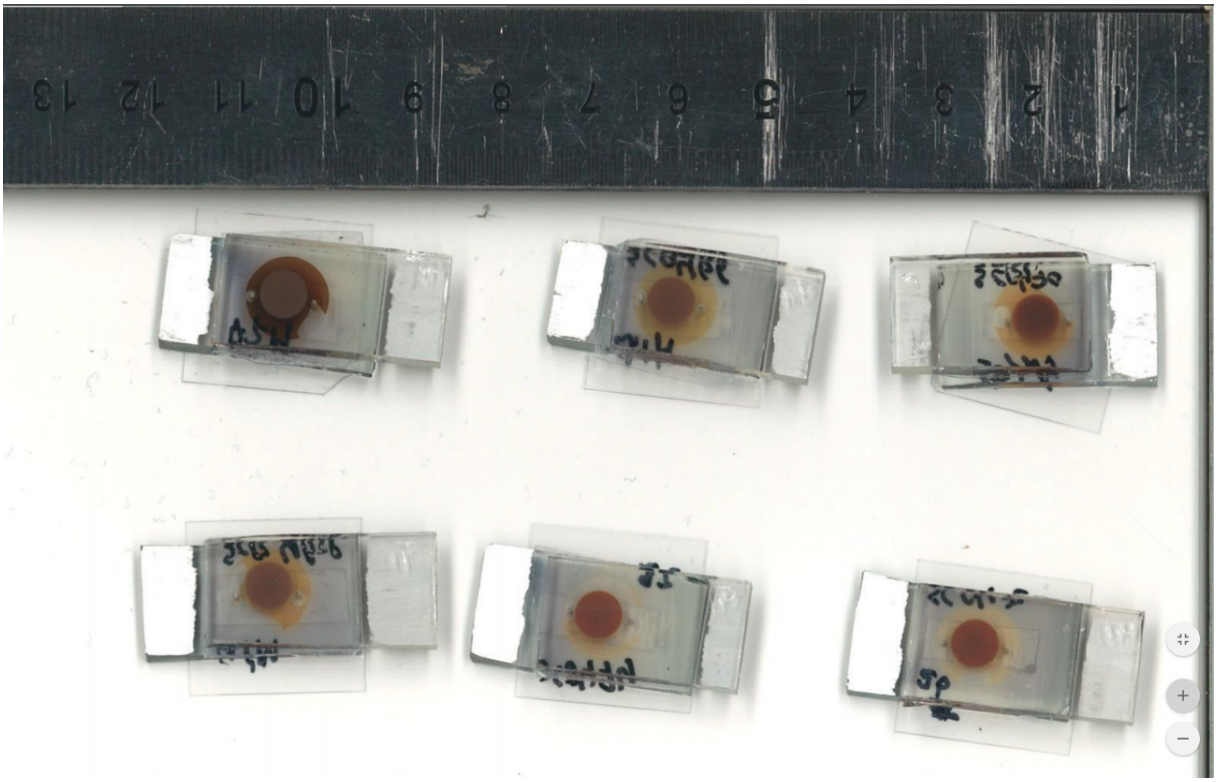

Figure S32. DSSCs under study to determine the average surface area of NiO. The average surface area was determined to be 0.196 ± 0.001 cm^{-2} using ImageJ to count the pixels.

S3. References

1. Pavlishchuk, V. V. & Addison, A. W. Conversion constants for redox potentials measured versus different reference electrodes in acetonitrile solutions at 25°C. *Inorganica Chim. Acta* **298**, 97–102 (2000).

2. Connelly, N. G. & Geiger, W. E. Chemical Redox Agents for Organometallic Chemistry. *Chem. Rev.* **96**, 877–910 (1996).

3. Hunter, C. A. & Anderson, H. L. What is cooperativity? *Angew. Chem. Int. Ed.* **48**, 7488–7499 (2009).

4. Bouwens, T., Mathew, S. & Reek, J. N. H. p-Type dye-sensitized solar cells based on pseudorotaxane mediated charge-transfer. *Faraday Discuss.* **215**, 393–406 (2019).

5. Fahrenbach, A. C. *et al.* Measurement of the ground-state distributions in bistable mechanically interlocked molecules using slow scan rate cyclic voltammetry. *Proc. Natl. Acad. Sci.* **108**, 20416–20421 (2011).

6. Wood, C. J. *et al.* A comprehensive comparison of dye-sensitized NiO photocathodes for solar energy conversion. *Phys. Chem. Chem. Phys.* **18**, 10727–10738 (2016).

7. Tian, H., Yu, Z., Hagfeldt, A., Kloo, L. & Sun, L. Organic redox couples and organic counter electrode for efficient organic dye-sensitized solar cells. *J. Am. Chem. Soc.* **133**, 9413–9422 (2011).

8. Yella, A. *et al.* Dye-sensitized solar cells using cobalt electrolytes: the influence of porosity and pore size to achieve high-efficiency. *J. Mater. Chem. C* **5**, 2833–2843 (2017).

9. Fabregat-Santiago, F., Garcia-Belmonte, G., Mora-Seró, I. & Bisquert, J. Characterization of nanostructured hybrid and organic solar cells by impedance spectroscopy. *Phys. Chem. Chem. Phys.* **13**, 9083 (2011).

10. Huang, Z., Natu, G., Ji, Z., Hasin, P. & Wu, Y. p-Type Dye-Sensitized NiO Solar Cells: A Study by Electrochemical Impedance Spectroscopy. *J. Phys. Chem. C* **115**, 25109–25114 (2011).

11. Benazzi, E., Mallows, J., Summers, G. H., Black, F. A. & Gibson, E. A. Developing photocathode materials for p-type dye-sensitized solar cells. *J. Mater. Chem. C* **7**,

10409–10445 (2019).

12. Powar, S. *et al.* Improved photocurrents for p-type dye-sensitized solar cells using nano-structured nickel(ii) oxide microballs. *Energy Environ. Sci.* **5**, 8896–8900 (2012).